Chalcogenide Letters

Tech Science Press

http://doi.org/10.32604/cl.2026.085371

ARTICLE

The Effect of Washing on the Structural, Morphological, and Compositional Properties of CuS Nanopowder Synthesis via Chemical Bath Technique

Bilal Taher*

College of Agriculture, University of Anbar, Ramadi, Iraq
*Corresponding Author: Bilal Taher. Email: ag.bilal.yaseen@uoanbar.edu.iq

Received: 10 May 2026; Accepted: 20 July 2026; Published: 07 August 2026

ABSTRACT: Nanopowder copper sulphide CuS has been synthesised successfully via the chemical bath deposition method. Two samples of precipitated CuS nanopowder were prepared at molar concentration of 0.5 M from [$CuSO_4{\cdot}5H_2O$ and $Na_2S_2O_3{\cdot}5H_2O$] and 0.05 M from [$Na_2EDTA{\cdot}2H_2O$]. Both samples were annealed at 150°C for one hour in air. The effects of washing and nonwashing on the structural, morphological, and compositional properties were studied. The X-ray diffraction (XRD) patterns showed that both samples have a CuS hexagonal structure with lattice constants (a = 3.773 Å, c = 16.398 Å), and (a = 3.792 Å, c = 16.534 Å), also the average crystallite size was found (11.4 nm, 4.5 nm) without washing and washing, respectively. Secondary phases Na_2EDTA-Cu complex impurity, $CuSO_4{\cdot}5H_2O$ and Cu_2O were showed in both samples and the intensity of peaks were reduced after washing. Field emission scanning electron microscopy (FESEM) analysis showed that the precipitated nanopowder has aggregated into hollow microsphere-like structures, resembling Bucky spheres, with average nanoparticle sizes of 62 nm and 58 nm for n-CuS and w-CuS, respectively. EDS analysis showed real and secondary phase values (15% and 85%) for the precipitated nanopowder without and with washing, respectively. The obtained results CuS nanopowder with high purity can be utilised in various photovoltaic applications.

KEYWORDS: CuS; nanopowder; synthesised; washing effect; properties; phase; CBD

1 Introduction

The importance of CuS nanopowder in the last years come through the using in the wide applications for different technological fields such as: light emitting [1], supercapacitor [2], treatment and purification of water and air [3,4], diverse biological uses and treatment [5–7], pharmaceutical and industrial [8], photocatalytic [9], photoelectrodes material in photovoltaic [10], solar cells [11], antibacterial device [12,13], optoelectronic [14], ammonia gas sensor [15], photoelectrochemical water splitting [16]. There are many methods to prepare CuS powder such as: wet chemical route [17,18], solvothermal method [19–21], hydrothermal method [22], magnetic grinding method [23], solid state grinding method [24], industrial milling [25], facile one pot microwave assisted [26], facile chemical conversion, double crucible sulfurisation [27], precipitation reaction [28], and precipitated from chemical bath deposition method [29–32]. It is known that the CBD technique was used to prepare thin films on the substrates. Regardless of whether the films are deposited on the substrates, the remaining solution after the experiment is discarded, resulting in a significant loss of the prepared solution in each experiment. In this study, the entire solution was utilised to produce pure nanopowder with minimal loss. In this study, the washing process was one of the purification methods used to remove unwanted impurities and surface contamination from the synthesised

nanopowder [33]. The effect of washing on the structural, morphological, and compositional properties of the prepared CuS nanopowder was studied.

2 Experimental Details

The procedure of all prepared solutions of nanopowder such as solutions, molar concentrations, sources of copper sulphate, sodium thiosulphate, EDTA complex agent, and characterisation techniques which were used to test the structural, morphological, and concentration ratios of precipitated CuS nanopowder were mentioned in previous our paper in details [34]. The best synthesised parameters have been applied in this study (deposition time 45 min, water bath temperature 50°C, and pH 2). All details of the experimental procedure are illustrated in the following flowchart Scheme 1.

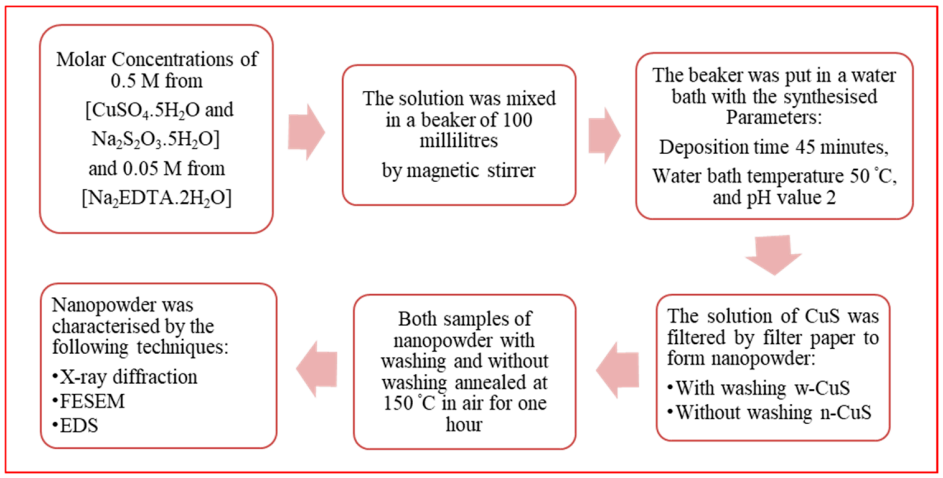

Scheme 1: The flowchart represents the experimental procedure for synthesising the CuS nanopowder in this work.

The prepared nanopowder samples are symbolised as "w-CuS and n-CuS", indicating the washed and unwashed samples, respectively.

The prepared solution was slowly filtered through filter paper to obtain nanopowder. For the first sample, n-CuS, the nanopowder was lifted without washing; for the second sample, w-CuS, it was washed.

The washing method for precipitated nanopowder included six total times: two with absolute chilled distilled water, two with a mixed solution of 50% ethanol and 50% distilled water, and two with absolute ethanol.

A wash bottle was used to carefully spray the washing solution onto the precipitate nanopowder to prevent nanoparticles loss.

After each washing process, the precipitate was allowed to settle by gravity for 10 to 20 min, and the supernatant was decanted. The nanopowders from both samples were annealed at 150°C for 1 h in air. The percentage value of the yield was 98% and 91.59% for n-CuS and w-CuS, respectively.

In this study, the effects of washing and nonwashing on the structural, morphological, and compositional properties of precipitated CuS nanopowder were investigated.

3 Results and Discussion

3.1 X-Ray Diffraction Analysis

XRD patterns of precipitated CuS nanopowder without washing (n-CuS) and with washing (w-CuS) are shown in Fig. 1. Both without washing and with washing of CuS nanopowder revealed a hexagonal covellite

nanostructure. The number of peaks of XRD patterns, and crystallographic planes for without washing n-CuS nanopowder indexed along (101), (102), (006), (103), (105), (110), (108), (116), and for washing w-CuS nanopowder indexed along (101), (102), (006), (110), (116) which belong to the hexagonal crystal structure of CuS according to JCPDS card No. 06-0464. Peaks at 2θ = 13.92, 18.48, 22.45 and 34.8° which corresponding Miller indices (002), (111), (112) and (220) in the XRD pattern for n-CuS indicate the presence of secondary phase Na_2EDTA-Cu complex impurity according to the ICDD card No. 00-050-2051 and $CuSO_4 \cdot 5H_2O$ with 2θ = 17.19, 24 and 26° which corresponding Miller indices (111), (020) and (120) according to the JCPDS 01-077-1900 which may be unreacted, and this occurs on the surface of the nanopowder before washing and the intensity reduce after washing. Also, the (311) and (222) peak at 2θ = 73.8 and 77.5° in both n-CuS and w-CuS indicates a secondary phase Cu_2O according to the JCPDS card No. 05-0667, due to partial oxidation or initial precursor ratios.

There are two main diffraction preferred peaks with high intensity corresponding to the Miller indices (103) and (110). From Fig. 1, the high intensity corresponding to (103) in sample n-CuS, which changes to (110) in sample w-CuS, means changing the preferred orientation plane because the precipitated nanopowder was affected by the washing, where any residual salts, ionic impurities, unreacted precursors, and contamination were removed, and the resultant nanopowder has been purified.

Also, the number of low intensity peaks in the sample w-CuS after washing is reduced, due to the enhanced in crystallinity of the prepared nanopowder.

Crystallite size (C.S) for both samples was calculated by using the Debye-Scherrer formula [35]

$$\mathrm{C.S} = \frac{0.9\lambda}{\beta \cos\theta} \tag{1}$$

where $\lambda = 0.154$ nm is the wavelength of the CuKα X-ray, θ is the Bragg angle (half of the diffraction angle 2θ) at which the peak is located, β is the full width at half maximum (FWHM) of the diffraction peak.

Lattice constants (a = b), and c for both samples, are calculated by the following equation [36]

$$\frac{1}{d^2} = \frac{4}{3}\left[\frac{h^2 + hk + k^2}{a^2}\right] + \frac{l^2}{c^2} \tag{2}$$

where d is the interplanar spacing lattice distance (Å), (hkl) are Miller indices, and (a and c) are lattice constants in (Å).

2θ for standard and experimental values, FWHM, d-spacing, Relative intensity %, Miller indices (hkl), and crystallite size (C.S) are tabulated in Tables 1 and 2 for without washing n-CuS, and with washing w-CuS, respectively.

Lattice constants were calculated as (a = 3773, c = 16.398) Å, and (a = 3.792, c = 16.534) Å for sample n-CuS and w-CuS, respectively. The lattice constants are in very good agreement with previous studies [37,38]. The lattice constants for the sample w-CuS with washing are greater than those of the sample n-CuS without washing, due to residual strain, defects or compositional variations rather than increased crystallinity of the prepared nanopowder. The average crystallite sizes were found as to be 11.4 nm, and 4.5 nm for n-CuS and w-CuS, respectively. These values of C.S are lower than those reported [39–41], and agree with those reported [42,43] in previous studies. The crystallite size decreases due to the washing effect which removes or reduces agglomeration, impurities, capping agents, and surface contaminants on the prepared nanopowder [44].

Table 1: Comparison of 2θ values for (standard and experimental), FWHM, d-spacing, Relative intensity %, Miller indices (hkl), and crystallite size (C.S) for the unwashed n-CuS sample.

2θ Standard	2θ Exp.	FWHM	d-Spacing [Å]	Rel. Int. Sta. [%]	Rel. Int. Exp. [%]	hkl	C.S nm
27.68	27.250	0.7872	3.2699	24	56.09	101	10.268
29.27	29.469	0.5904	3.0285	54	69.4	102	13.758
31.78	31.688	0.492	2.8213	90	100	103	16.598
47.93	48.202	0.5904	1.8863	100	84.85	110	14.577
52.71	53.267	1.5744	1.7183	51	19.62	108	5.582
59.34	59.494	1.2	1.5524	57	37.52	116	7.540

Table 2: Comparison of 2θ values for (standard and experimental), FWHM, d-spacing, Relative intensity %, Miller indices (hkl), and crystallite size (C.S) for the washed w-CuS sample.

2θ Standard	2θ Exp.	FWHM	d-Spacing [Å]	Rel. Int. Sta. [%]	Rel. Int. Exp. [%]	hkl	C.S nm
29.27	28.953	2.9673	3.0813	54	48.3	102	2.734
31.78	32.112	1.472	2.7850	90	84.87	103	5.553
47.93	47.943	1.1348	1.8959	100	100	110	7.576
59.43	59.096	3.8515	1.5619	57	31.6	116	2.344

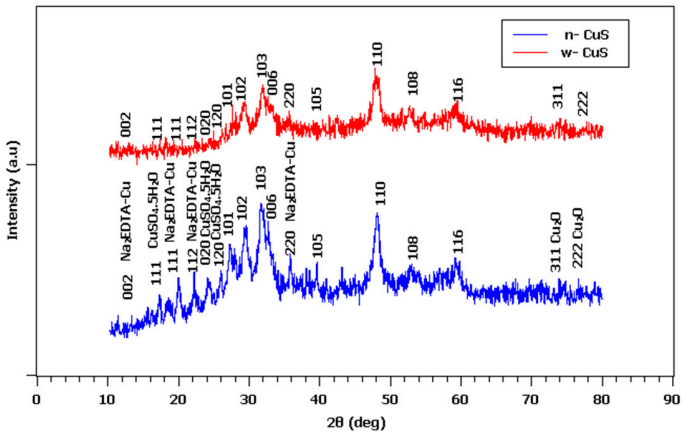

Figure 1: XRD patterns for CuS nanopowder without washing (n-CuS) and with washing (w-CuS).

3.2 Surface Morphological Analysis

3.2.1 FESEM Characterization

Morphological properties of precipitated CuS nanopowder were characterised by field emission scanning electron microscopy (FESEM). Images of precipitated CuS nanopowder (without washing n-CuS and with washing w-CuS) are shown in Figs. 2 and 3, respectively. it is clear the nanoparticles in both samples n-CuS and w-CuS have been aggregated with hollow microspheres like structures which agreement with [45], and the aggregation of nanoparticles like as a Bucky spheres with thin shell, these microspheres were bonded between them such as hexagonal structure, and in the sample w-CuS the formed nanoparticles with the hexagonal structure have been observed with more purity in microstructure compare with that in the sample n-CuS, and this was observed in diffraction patterns in XRD analysis. In fact, the nanopowder consists of many nanoparticles, and each nanoparticle consists of many tiny primary nanoparticles. FESEM images, the nanoparticles in both n-CuS and w-CuS nanopowder are composed of many grains or primary

nanoparticles that agglomerate to form nanoparticles or polycrystalline spheres. Fig. 4 shows the nanoparticle size distribution, indicating that w-CuS has a higher proportion of smaller nanoparticles compared to n-CuS. The average nanoparticles sizes are 62 nm for n-CuS and 58 nm for w-CuS. Consequently, the average nanoparticle exceeds the crystallite size determined by XRD analysis. Additionally, nanoparticle agglomeration is more pronounced in w-CuS than in n-CuS nanopowder. All nanoparticles sizes were analysed and determined by using the free ImageJ program.

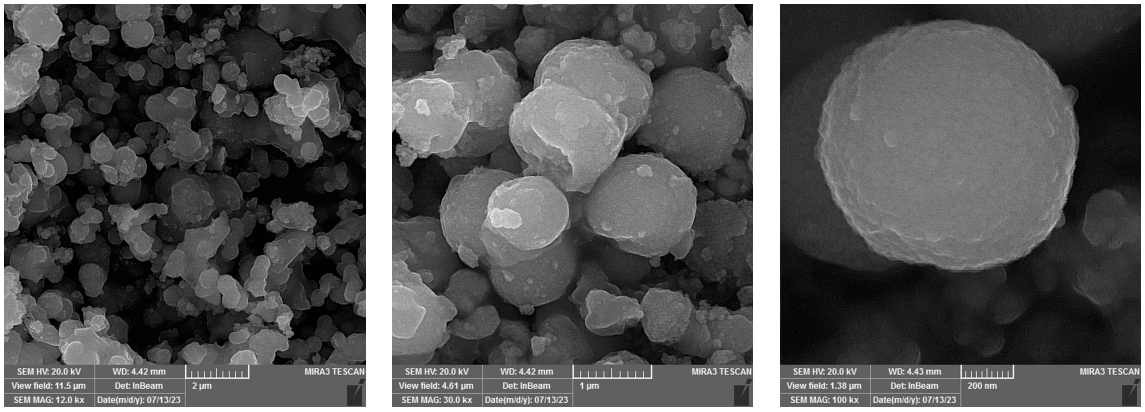

Figure 2: FESEM images with scale (2 µm, 1 µm, and 200 nm) for CuS nanopowder without washing n-CuS.

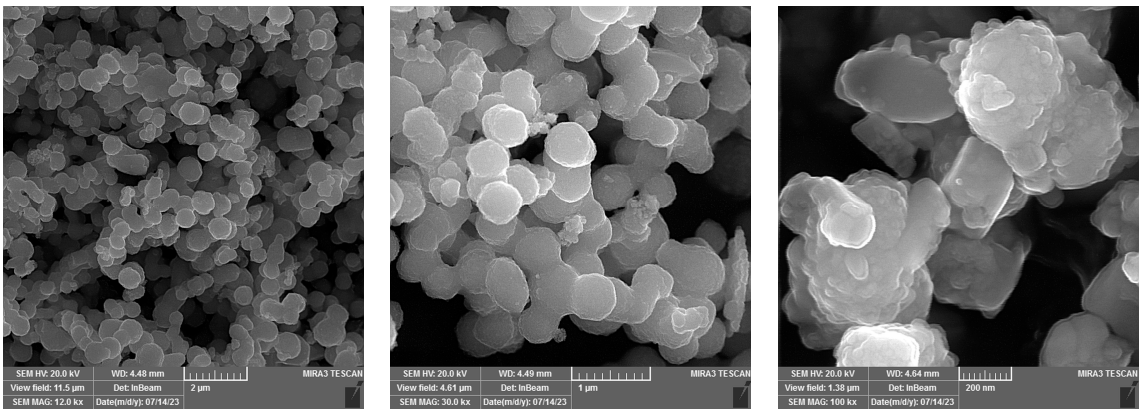

Figure 3: FESEM images with scale (2 µm, 1 µm, and 200 nm) for CuS nanopowder with washing w-CuS.

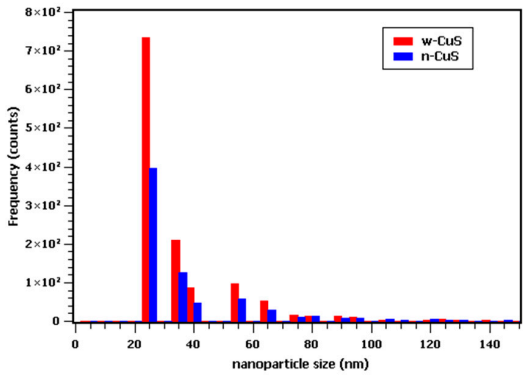

Figure 4: Distribution of nanoparticle size for CuS nanopowder without washing (n-CuS) and with washing (w-CuS).

3.2.2 Compositional Analysis

The elemental compositions, the colour map of element distribution, and the SEM images obtained by EDS analysis are shown in Fig. 5. The percentage ratio (%) of the prepared nanopowder was taken only for elements that form the CuS nanopowder. The other elements O, C and Cl were found in both samples of prepared nanopowder due to the precipitated nanopowder technique in air. The percentage ratio (%) of elements Cu and S only was calculated through (Atomic At%) in Table 3. The precipitated nanopowders n-CuS (without washing) and w-CuS (with washing), showed real-phase values of 15%, which agree with the XRD pattern analysis. The best precipitated nanopowder was obtained after washing, indicating greater crystallisation of the formed nanopowder.

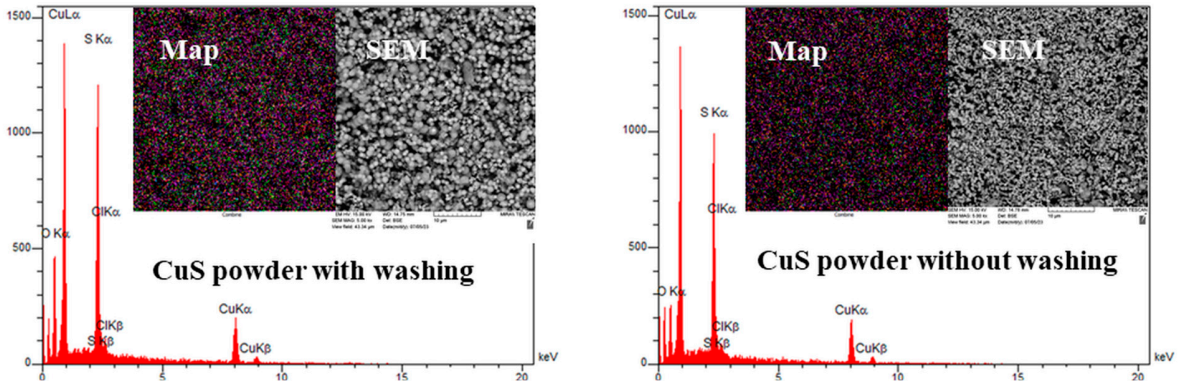

Figure 5: EDS plot included compositions of elements, a map for distribution of formed nanopowder, and an SEM image with scale (10 μm) of elements for CuS nanopowder with washing and without washing.

Table 3: Compositions of nanopowder, and ratio of real and secondary phases of formed CuS nanopowder from EDS analysis.

Sample	At% of CuS Total Powder					At% of CuS Formed Powder		Formula	Real Phase %	Secondary Phase %
	Cu	S	C	O	Cl	Cu	S			
n-CuS	7.63	8.72	49.42	33.66	0.57	0.076	0.087	$Cu_{0.15}S_{0.17}$	15	85
w-CuS	7.40	7.43	62.35	22.2	0.62	0.074	0.074	$Cu_{0.15}S_{0.15}$	15	85

4 Conclusions

In this work, CuS nanopowder was precipitated using the CBD technique. The effects of washing and nonwashing on the structural, morphological, and compositional properties of precipitated CuS nanopowder were studied. The conclusion of the results is based on the following:

Both washed and unwashed CuS nanopowders revealed a hexagonal covellite nanostructure. Lattice constants were found as (a = 3773, c = 16.398) Å, and (a = 3.792, c = 16.534) Å, and the average crystallite size was found as 11.4 nm, and 4.5 nm for CuS nanopowder without washing and with washing, respectively.

Secondary phases common in the CBD technique come from varied stoichiometry of copper or sulphur, and oxygen in air can lead to the formation of Cu_2S, $CuSO_4{\cdot}5H_2O$ and Na_2EDTA-Cu complex, and the intensity of these secondary phases reduce after the washing process.

Precipitated nanopowder has been aggregated into hollow microsphere-like structures, termed Bucky spheres, with a thin shell, without washing and with washing, respectively, using CuS nanopowder. The average nanoparticles sizes are 62 nm for n-CuS and 58 nm for w-CuS.

The precipitated CuS nanopowder, both without and with washing, showed real and secondary phase values of 15% and 85%, respectively.

The two processes without and with washing are of high purity, but the process with washing was more pure and had more advantages in different applications.

In this study, the entire solution was used to produce pure nanopowder with minimal loss; therefore, the resulting CuS nanopowder with high purity can be utilised in various photovoltaic applications.

Acknowledgement: I would like to thank the Central lab in my College of Agriculture, University of Anbar, for helping me to complete this work.

Funding Statement: The author received no specific funding for this study.

Availability of Data and Materials: The data supporting the findings of this study are available from corresponding author upon reasonable request.

Ethics Approval: Not applicable.

Conflicts of Interest: The author declares no conflicts of interest.

References

1. Sabah FA, Abdul Razak I, Kabaa EA, Zaini MF, Omar AF. Influence of CuS powder concentration on the construction of hybrid PVA/CuS thin films for polymer light-emitting applications. J Mater Sci Mater Electron. 2020;31(4):3456–65. [CrossRef].
2. Singhal R, Thorne D, LeMaire PK, Martinez X, Zhao C, Gupta RK, et al. Synthesis and characterization of CuS, CuS/graphene oxide nanocomposite for supercapacitor applications. AIP Adv. 2020;10(3):035307. [CrossRef].
3. Bordunov SV, Galtseva OV, Natalinova NM, Rogachev AA, Zhang R. Physico-chemical modification of the fibrous filter nozzles for purification processes of water and air. IOP Conf Ser Mater Sci Eng. 2017;168(1):012087. [CrossRef].
4. Yu S, Liu J, Zhu W, Hu ZT, Lim TT, Yan X. Facile room-temperature synthesis of carboxylated graphene oxide-copper sulfide nanocomposite with high photodegradation and disinfection activities under solar light irradiation. Sci Rep. 2015;5:16369. [CrossRef].
5. Muhsen MM, Al-Jawad SMH, Taha AA. NIR laser-conjugated glutathione-coated Mn-doped CuS nanoprisms as photothermal agent for cancer treatment. Lasers Med Sci. 2022;38(1):15. [CrossRef].
6. Argueta-Figueroa L, Martínez-Alvarez O, Santos-Cruz J, Garcia-Contreras R, Acosta-Torres LS, de la Fuente-Hernández J, et al. Nanomaterials made of non-toxic metallic sulfides: A systematic review of their potential biomedical applications. Mater Sci Eng C Mater Biol Appl. 2017;76:1305–15. [CrossRef].
7. Wang X, Yang Z, Meng Z, Sun SK. Transforming commercial copper sulfide into injectable hydrogels for local photothermal therapy. Gels. 2022;8(5):319. [CrossRef].
8. Zhang L, Chen M, Jiang Y, Chen M, Ding Y, Liu Q. A facile preparation of montmorillonite-supported copper sulfide nanocomposites and their application in the detection of H_2O_2. Sens Actuators B Chem. 2017;239:28–35. [CrossRef].
9. Kao YT, Yang SM, Lu KC. Synthesis and photocatalytic properties of CuO-CuS core-shell nanowires. Materials. 2019;12(7):1106. [CrossRef].
10. Chen F, Zhu X, Fan X, Liu H, Pan W, Zhou X, et al. Hierarchical CuS Nanoflowers enable efficient photo-assisted Cu^{2+} reversible storage for advanced aqueous copper ion batteries. Adv Powder Technol. 2026;37(2):105160. [CrossRef].
11. Mezgebe MM, Ju A, Wei G, Macharia DK, Guang S, Xu H. Structure based optical properties and catalytic activities of hydrothermally prepared CuS nanostructures. Nanotechnology. 2019;30(10):105704. [CrossRef].
12. Liu Z, Liu Q, He X, Zhu Y, Pan Q, Zhang R, et al. Polydopamine and CuS/$CaCO_3$ nanocomposites coated titanium alloy screw as efficient antibacterial device. Vacuum. 2023;214:112208. [CrossRef].

13. Mohanty A, Patra S, Bhutia SK, Mohapatra S. Skin-adhesive antibacterial hydrogel loaded with biosynthesized CuS nanoparticles for NIR laser-induced wound healing. ACS Appl Bio Mater. 2026;9(1):412–22. [CrossRef].
14. Muhi MAH, Gbashi KR, Salih AT, Najim AA. Novel covellite CuS single-crystal thin films for optoelectronic applications. Plasmonics. 2018;13(1):247–50. [CrossRef].
15. Xu J, Zhang J, Yao C, Dong H. Synthesis of novel highly porous CuS golf balls by hydrothermal method and their application in ammonia gas sensing. J Chil Chem Soc. 2013;58(2):1722–4. [CrossRef].
16. Heidari G, Rabani M, Ramezanzadeh B. Application of CuS–ZnS PN junction for photoelectrochemical water splitting. Int J Hydrogen Energy. 2017;42(15):9545–52. [CrossRef].
17. Tailor JP, Chaki SH, Deshpande MP. Comparative study between pure and manganese doped copper sulphide (CuS) nanoparticles. Nano Express. 2021;2(1):010011. [CrossRef].
18. Goswami M, Nithya C, Sathish N, Kumar S, Singh N, Srivastava AK, et al. Electrochemical studies on crystalline CuS as an electrode material for non-aqueous Na-ion capacitors. New J Chem. 2020;44(14):5278–84. [CrossRef].
19. Zhang X, Gao Y, Li Y, Zhou Y, Ma H, Shang J, et al. Synthesis of magnetic $NiFe_2O_4$/CuS activator for degradation of lomefloxacin via the activation of peroxymonosulfate under simulated sunlight illumination. Sep Purif Technol. 2022;288:120664. [CrossRef].
20. Shaabanzadeh Z, Khorshidi A, Moafi HF, Tabatabaeian K. CuS NPs/zeolite A/ZIF-8 dual-action composite for removal of methylene blue from aqueous solutions. J Cluster Sci. 2023;34(1):487–99. [CrossRef].
21. Das M, Das D, Sil S, Ray PP. Development of hierarchical copper sulfide-carbon nanotube (CuS-CNT) composites and utilization of their superior carrier mobility in efficient charge transport towards photodegradation of Rhodamine B under visible light. Nanoscale Adv. 2023;5(14):3655–63. [CrossRef].
22. Kumar S, Ganguli AK. Enhanced photoelectrochemical water splitting and mitigation of organic pollutants under visible light with $NaNbO_3$@CuS Core-Shell heterostructures. Appl Surf Sci Adv. 2022;9:100239. [CrossRef].
23. Song Z, Liu Y, Zhang B, Song S, Zhou Z, Huang Y, et al. Magnetic grinding synthesis of copper sulfide-based photocatalytic composites for the degradation of organic dyes under visible light. New J Chem. 2023;47(5):2286–95. [CrossRef].
24. Bera A, Busupalli B, Prasad BLV. Solvent-less solid state synthesis of dispersible metal and semiconducting metal sulfide nanocrystals. ACS Sustain Chem Eng. 2018;6(9):12006–16. [CrossRef].
25. Achimovičová M, Dutková E, Tóthová E, Bujňáková Z, Briančin J, Kitazono S. Structural and optical properties of nanostructured copper sulfide semiconductor synthesized in an industrial mill. Front Chem Sci Eng. 2019;13(1):164–70. [CrossRef].
26. Mahalingam S, Ayyaru S, Ahn YH. Facile one-pot microwave assisted synthesis of rGO-CuS-ZnS hybrid nanocomposite cathode catalysts for microbial fuel cell application. Chemosphere. 2021;278:130426. [CrossRef].
27. Cheng L, Li D, Yu W, Ma Q, Dong X, Wang X, et al. A novel strategy to fabricate CuS, $Cu_{7.2}S_4$, and $Cu_{2-x}Se$ nanofibers via inheriting the morphology of electrospun CuO nanofibers. Russ J Phys Chem. 2019;93(4):730–5. [CrossRef].
28. Rao P, Kumar S, Raje N, Tokas RB, Sahoo NK. Synthesis of binary and multinary metal sulphides by precipitation and their characterisation. Mater Res Bull. 2016;79:105–14. [CrossRef].
29. Pejjai B, Reddivari M, Kotte TRR. Phase controllable synthesis of CuS nanoparticles by chemical co-precipitation method: Effect of copper precursors on the properties of CuS. Mater Chem Phys. 2020;239:122030. [CrossRef].
30. Manwai CF, Kalita PK, Das H. Optoelectronic properties of CuS nanoparticles for potential application in memory devices. Phys Status Solidi A. 2026;223:e202500658. [CrossRef].
31. Hu H, Gomez-Daza O, Baños L. Screen printed conductive CuS-poly(acrylic acid) composite coatings. Sol Energy Mater Sol Cells. 1998;56(1):57–65. [CrossRef].
32. Hu H, Campos J, Nair PK. Electrically conductive CuS–poly(acrylic acid) composite coatings. J Mater Res. 1996;11(3):739–45. [CrossRef].
33. Miyamoto R, Amari S, Takiyama H. Comparison of the effects of crystalline particle size modified by crystallization on the mother liquor removal profiles of washing and reslurry. J Chem Eng Jpn. 2023;56:2206851. [CrossRef].
34. Taher B. Structural, morphological, compositional and optical properties of copper sulphide thin films prepared by chemical bath deposition technique. In: Proceedings of the 2nd Joint International Conference on Mathematics, Statistics and Engineering: J-CoMSE2024; 2025 Sep 17–18; Kedah, Malaysia. [CrossRef].

35. Ghribi F, Alyamani A, Ben Ayadi Z, Djessas K, EL Mir L. Study of CuS thin films for solar cell applications sputtered from nanoparticles synthesised by hydrothermal route. Energy Procedia. 2015;84:197–203. [CrossRef].
36. Al-Hammadi AH, Al-Adhreai AA, Abdulwahab AM, Al-Adhreai A, Salem A, Alaizeri ZM, et al. An investigation on the structural, morphological, optical, and antibacterial activity of Sr:CuS nanostructures. Sci Rep. 2024;14:25169. [CrossRef].
37. Deb S, Kalita PK. Green synthesis of copper sulfide (CuS) nanostructures for heterojunction diode applications. J Mater Sci Mater Electron. 2021;32(19):24125–37. [CrossRef].
38. Ou S, Xie Q, Ma D, Liang J, Hu X, Yu W, et al. A precursor decomposition route to polycrystalline CuS nanorods. Mater Chem Phys. 2005;94(2–3):460–6. [CrossRef].
39. Goswami M, Kumar S, Siddiqui H, Atram L, Singh N, Prasad HC, et al. Morphology variations in copper sulfide nanostructures as anode materials for Na-ion capacitors. ACS Appl Nano Mater. 2023;6(17):15498–509. [CrossRef].
40. Hussein ON, AL-Jawad SMH, Imran NJ. A study on the influence of metal Fe, Ag, and Mn doping and (Fe/Mn and Ag/Mn) dual-doping on the structural, morphological, optical, and antibacterial activity of CuS nanostructures. Plasmonics. 2024;19(3):1101–20. [CrossRef].
41. Shanan ZJ, Majed MD, Ali HMJ. Effect of the concentration of copper on the properties of copper sulfide nanostructure. Baghdad Sci J. 2022;19(1):225. [CrossRef].
42. Hussein ON, AL-Jawad SMH, Imran NJ. Structural, morphological, optical, and antibacterial properties of Mn and (Ag, Mn) co-doped copper sulfide nanostructures. Opt Quantum Electron. 2023;55(6):503. [CrossRef].
43. Song DH, Song JH, Cho SB, Lim DY. Low-temperature synthesis of CuS nanopowders using a simple glycolate method. J Nanosci Nanotechnol. 2017;17(6):4352–5. [CrossRef].
44. Hassanzadeh-Tabrizi SA. Precise calculation of crystallite size of nanomaterials: A review. J Alloys Compd. 2023;968:171914. [CrossRef].
45. Liu Y, Zhou Z, Zhang S, Luo W, Zhang G. Controllable synthesis of CuS hollow microflowers hierarchical structures for asymmetric supercapacitors. Appl Surf Sci. 2018;442:711–9. [CrossRef].